

Terahertz pulse-driven collective mode in the nematic superconducting state of $\text{Ba}_{1-x}\text{K}_x\text{Fe}_2\text{As}_2$

Romain Grasset^{1,2,3}, Kota Katsumi², Pierre Massat⁴, Hai-Hu Wen⁵, Xian-Hui Chen⁶, Yann Gallais^{1,2,4}
& Ryo Shimano^{1,2}

¹*Cryogenic Research Center, The University of Tokyo, Tokyo, 113-0032, Japan*

²*Department of Physics, The University of Tokyo, Tokyo, 113-0033, Japan*

³*Laboratoire des Solides Irradiés, Ecole Polytechnique, CNRS, CEA, Institut Polytechnique de Paris, F-91128 Palaiseau, France*

⁴*Laboratoire Matériaux et Phénomènes Quantiques, UMR 7162 CNRS, Université de Paris, Bât. Condorcet 75205 Paris Cedex 13, France*

⁵*National Laboratory of Solid State Microstructures and Department of Physics, Nanjing University, Nanjing 210093, China*

⁶*Hefei National Laboratory for Physical Sciences at Microscale and Department of Physics, and CAS Key Laboratory of Strongly-coupled Quantum Matter Physics, University of Science and Technology of China, Hefei, Anhui 230026, China*

Abstract

We investigate the collective mode response of the iron-based superconductor $\text{Ba}_{1-x}\text{K}_x\text{Fe}_2\text{As}_2$ using intense terahertz (THz) light. In the superconducting state a THz Kerr signal is observed and assigned to non-linear THz coupling to superconducting degrees of freedom. The

polarization dependence of the THz Kerr signal is remarkably sensitive to the coexistence of a nematic order. In the absence of nematic order the C_4 symmetric polarization dependence of the THz Kerr signal is consistent with a coupling to the Higgs amplitude mode of the superconducting condensate. In the coexisting nematic and superconducting state the signal becomes purely nematic with a vanishing C_4 symmetric component, signaling the emergence of a new superconducting collective mode activated by nematicity.

Introduction

Superconductivity with coexisting electronic orders can be found in various strongly correlated systems. Among these orders electron nematics, where the electron fluid breaks the discrete rotational symmetry of the underlying lattice, have recently emerged as an ubiquitous phase in many superconductors ranging from cuprates ¹, to iron-based superconductors ² where superconductivity emerges within a nematic phase, and more recently doped Bi_2Se_3 ³ and twisted bi-layer graphene ^{4,5} where the superconductivity itself may have a nematic component. In iron-based superconductors (Fe SC), superconductivity is found to coexist with both stripe-like magnetic spin-density-wave (SDW) and nematic orders. BaFe_2As_2 , a member of this family, undergoes a nematic-structural transition from a C_4 to a C_2 symmetric phase, followed by a SDW transition ^{2,6}. The C_4 rotational symmetry breaking is triggered by electronic degrees of freedom and has been dubbed nematic for this reason ^{2,7,8}. With increasing doping by substitution (e.g. Ba with K or Fe with Co ^{6,9}), the C_2 symmetric nematic-SDW phase, hereafter called the C_2 phase, is weakened and a superconducting (SC) dome forms around a possible quantum critical point. The

coexistence with the C_2 phase can profoundly impact the nature of SC order, by coupling different nearly degenerate pairing channels like s and d wave^{10,11}, or inducing an orbitally-selective SC state^{12,13}.

One way to gain insight into the coupling between nematic and SC degrees of freedom is to study the collective modes of the SC state upon entering the C_2 SC phase. Theoretically, intertwined electronic orders where superconductivity coexists with other electronic orders can lead to a rich spectrum of SC collective modes^{14–16,16–24}. In a single band conventional superconductor the collective mode excitation spectrum consists of two modes: the Nambu-Goldstone phase mode which is shifted to the plasma frequency through the Anderson-Higgs mechanism, and the Higgs amplitude mode located at twice the SC gap energy. The Higgs mode does not couple linearly to light^{14,25,26}. Except in very special cases like charge-density-wave superconductors^{27–30}, its observation has remained elusive until very recently. In this context, strong terahertz (THz) pulses have emerged as a tool of choice because they can access hidden SC collective modes via non-linear optical processes^{31–35,35–37}. This has led to the observation of the SC Higgs mode in several SC materials like NbN and Nb₃Sn, but also in cuprates and Fe SC^{38–45}. In the case of Fe SC however, little is known experimentally about the impact of nematicity on SC collective modes like the Higgs.

Here we investigate the THz non-linear response of the Fe SC Ba_{1-x}K_xFe₂As₂ where superconductivity coexists with a nematic order using a THz pump near-infrared (NIR) probe scheme. In the SC state, we observe an instantaneous response which follows the square of the THz electric

field which is assigned to the non-linear THz Kerr effect. In the absence of a coexisting nematic order the THz Kerr signal displays a C_4 symmetric polarization dependence consistent with a non-linear coupling to the SC Higgs mode. In the presence of a coexisting nematic order, the THz Kerr signal displays a drastic change in its polarization dependence: from fully-symmetric in the C_4 symmetric SC phase to fully nematic in the C_2 symmetric phase. We show theoretically that the onset of the THz Kerr Higgs response in the nematic channel can be qualitatively explained by taking into account the anisotropy of the electronic structure in the C_2 nematic phase. However, the complete disappearance of the C_4 symmetric signal in the C_2 SC phase cannot be captured within this simple picture, indicating a non-trivial interplay between the nematic and superconducting order parameters and the emergence of a new collective mode, distinct from the Higgs mode. We tentatively assigned this mode to the Bardasis-Schrieffer mode connecting s-wave and d-wave superconducting ground states which become mixed in the C_2 symmetric SC phase.

Results

Non-linear THz Kerr effect. We studied two single crystals of $\text{Ba}_{1-x}\text{K}_x\text{Fe}_2\text{As}_2$ with $T_c = 26\text{K}$ (UD26) and $T_c = 37\text{K}$ (UD37). The UD26 crystal is slightly underdoped and exhibits a simultaneous nematic/SDW transition at $T_N \sim T_S \sim 90\text{K}$. The UD37 crystal only exhibits a superconducting transition and is close to optimal doping. The terahertz-pump optical reflectivity probe (TPOP) measurement scheme is depicted in Figure 1(a). Measurements were carried out with a fixed THz pump polarization along the Fe-Fe direction but two different probe polarizations either parallel or perpendicular to the pump polarization (Figure 1(b)). Fe-Fe directions are identified by

a 45° tilt with respect to the edges of the crystals which are square-shaped.

In Figure 1(c,d) we compare the THz pump spectrum with the SC state Raman spectra of the two samples ⁴⁶. With an energy centered around $\omega_p=0.6$ THz= 20 cm⁻¹, the THz pump spectrum is located below the lowest superconducting gap $2\Delta_h$ observed by Raman scattering. Based on previous Raman and angle-resolved photoemission spectroscopy (ARPES) measurements this gap is assigned to the Γ centered hole pockets. The TPOP signal $\frac{\Delta R}{R}$ of UD37 below T_c is shown in Fig. 1(e). It consists of essentially two components, an instantaneous component that follows the square of the THz E -field (red line in Fig. 1(e)) and a broader decaying component which last several picoseconds after the pump pulse. In the following we will mostly focus on the instantaneous component, the THz Kerr effect, where the strong THz E field modulates the optical reflectivity in the NIR regime ⁴⁷. We note that in our measurements we only detect an instantaneous component that is proportional to the square of the THz E field, consistent with the centrosymmetric crystal structure of Ba_{1-x}K_xFe₂As₂. No forbidden odd contribution is observed, as recently reported in the SC state of NbN⁴⁸ and attributed to THz field symmetry breaking.

The THz Kerr signal is described by a third-order nonlinear susceptibility $\chi^{(3)}(\omega; \omega, +\Omega, -\Omega)$ ^{49,50}, where ω and Ω are the frequencies of the NIR pulse and THz-pump pulse, respectively. The THz pulse-induced reflectivity change $\Delta R/R$ can be expressed in terms of $\chi^{(3)}$ ⁴⁶ as

$$\frac{\Delta R}{R}(E_i^{probe}, E_j^{probe}) \sim \frac{1}{R} \frac{\delta R}{\delta \epsilon_1} \epsilon_0 [Re \chi_{ijkl}^{(3)}] E_k^{pump} E_l^{pump} \quad (1)$$

where E_i denotes the i th component of the THz-pump or probe E field and ϵ_1 is the real part of the dielectric constant at 1.5 eV. The instantaneous Kerr signal of interest here implies $\Omega=0$ in $\chi^{(3)}$.

It is therefore independent of the pump frequency Ω and non-resonant^{42,50}. This is in contrast with the Third-Harmonic Generation (THG) signal which is resonant when the pump frequency Ω equals the superconducting gap Δ ³¹.

In general, the onset of a THz Kerr signal below T_c can be assigned to two different processes: coupling to charge density fluctuations (CDF) like the one observed in Raman experiments, or to the SC Higgs mode. As previously shown in the case of NbN and cuprates important clues about the origin of the THz Kerr signal, and other third-order non-linear effects like THG, can be obtained by investigating its polarization dependence^{32,35,36,40,42,43}.

Assuming C_4 tetragonal symmetry for the normal state of $\text{Ba}_{1-x}\text{K}_x\text{Fe}_2\text{As}_2$, we can analyze the polarization dependence of $\chi^{(3)}(\theta_{pump}, \theta_{probe})$ in terms of the irreducible representations of D_{4h} point group as

$$\chi^{(3)}(\theta_{pump}, \theta_{probe}) = \frac{1}{2}(\chi_{A_{1g}}^{(3)} + \chi_{B_{1g}}^{(3)} \cos 2\theta_{pump} \cos 2\theta_{probe} + \chi_{B_{2g}}^{(3)} \sin 2\theta_{pump} \sin 2\theta_{probe}) \quad (2)$$

where we have defined the symmetry-resolved non-linear response functions: $\chi_{A_{1g}}^{(3)} = \chi_{aaaa}^{(3)} + \chi_{bbaa}^{(3)}$, $\chi_{B_{1g}}^{(3)} = \chi_{aaaa}^{(3)} - \chi_{bbaa}^{(3)}$ and $\chi_{B_{2g}}^{(3)} = \chi_{abab}^{(3)} + \chi_{abba}^{(3)}$. and $\theta_{probe/pump}$ are the angle between the probe/pump polarization vectors and the a axis of the 1 Fe unit cell. The A_{1g} is the fully symmetric representation and the B_{1g}/B_{2g} representation transform as $x^2 - y^2$ and xy respectively. The B_{1g} representation has the same symmetry as the C_2 symmetric nematic order parameter found in Fe SC. For $\theta_{pump}=0$, the A_{1g} and B_{1g} responses can be accessed using two distinct probe polarization

orientations. Indeed making use of equation 1 we can write:

$$\begin{aligned}\frac{\Delta R^{C_4}}{R} &= \frac{\Delta R_a}{R_a} + \frac{\Delta R_b}{R_b} \propto \text{Re}\chi_{A_{1g}}^{(3)} \\ \frac{\Delta R^{nem}}{R} &= \frac{\Delta R_a}{R_a} - \frac{\Delta R_b}{R_b} \propto \text{Re}\chi_{B_{1g}}^{(3)}\end{aligned}\quad (3)$$

where R_i ($i = a, b$) denotes the reflectivity for a probe polarization along the Fe-Fe axes (a,b) of Figure 1.b and for a fixed pump polarization along the a axis. Here we have taken $R_a = R_b$ (C_4 tetragonal symmetry). Since the notations B_{1g} and A_{1g} are no longer valid in the C_2 symmetric orthorhombic phase, we will adopt the notation " C_4 " for C_4 symmetric and "nem" for nematic (or C_2 symmetric) when discussing the results below.

Response in the C_4 symmetric superconducting state. We start by discussing the C_4 symmetric and nematic components of the TPOP signal of the UD37 crystal for which only superconductivity is present. Figure 2(a,b) show the transient reflectivity obtained for both C_4 symmetric and nematic components in the UD37 crystal and at various temperatures ranging from 15 K to 70 K. The decaying part of the $\Delta R/R$ signal shows a strong increase in the C_4 symmetric channel across T_c indicating the superconducting transition (Inset of Figure 3(a)). The instantaneous Kerr component is only observed below T_c , confirming it is linked to the onset of superconductivity. On the other hand, in the nematic channel no significant changes appear in the transient reflectivity at all temperatures. Using the fitting procedure displayed in Figure 2(e,g), we can obtain the temperature dependencies of the instantaneous and decaying components of $\frac{\Delta R^{C_4}}{R}$ and $\frac{\Delta R^{nem}}{R}$ (Figure 3(a)). The decaying component displays a sharp extremum around T_c and is assigned to the dynamical relaxation of quasi-particles (QP) in the SC state⁴⁶. The instantaneous component, attributed to the THz Kerr effect, shows a strong enhancement below T_c . The absence of the in-

stantaneous Kerr component in the nematic channel argues in favor of a contribution arising from the Higgs excitation. Indeed, as shown in the case of $\text{Bi}_2\text{Sr}_2\text{CaCu}_2\text{O}_{8+x}$ cuprates charge density fluctuations are expected to contribute to all symmetry channels whereas the Higgs contribution is only active in the fully-symmetric, i.e. C_4 symmetric for a tetragonal crystal, channel^{35,36,40,42,51}. Interestingly, Raman scattering spectra on the same crystal in the SC state are dominated by the B_{1g} channel^{11,46}, indicating they mostly probe CDF contributions in stark contrast with the THz Kerr signal. We note that the respective weight between Higgs and CDF contributions to third-order non-linear susceptibilities has been a subject of a debate since BCS calculations indicate dominant CDF contributions for a clean superconductor³². However, there is now an emerging consensus that disorder significantly boosts the Higgs contribution, thus giving a rationale to the dominance of the Higgs contribution observed in THz Kerr and THG experiments in all superconductors studied so far^{33,35,36,52,53}.

Response in the C_2 symmetric superconducting state. Having discussed the simple case of the C_4 symmetric superconductor case, let us now turn to the sample with a lower doping level, UD26 which display a C_2 symmetric SC phase with both nematic and SC orders. Figure 2(c,d) shows the transient reflectivity obtained for both channels and at various temperatures ranging from 9.5 K to 110 K. Above T_c , in contrast to UD37, both C_4 symmetric and nematic components show a change in the transient reflectivity below $T_{S/N} \sim 90$ K indicating the transition to the C_2 symmetric nematic phase. The onset of a decaying signal in the nematic channel is consistent with optical pump optical probe measurements on $\text{BaFe}_2(\text{As}_{1-x}\text{P}_x)_2$ which reported a similar strongly anisotropic signal below $T_{S/N}$ ⁵⁴. In principle, a mixture of C_2 domains of different orientation

would average out the nematic component of our signal. The fact that we observe a significant non-zero $\frac{\Delta R}{R}^{nem}$ shows that one domain orientation prevails under our 250 μm laser spot. We attribute this relatively large domain size to residual strains on the sample due to sample mounting which act as symmetric breaking field and align the nematic domains.

Below T_c , an instantaneous Kerr component of $\Delta R/R$ that follows the squared THz-pump E-field is also identified, with however a striking difference compared to UD37. Indeed, while it is essentially absent in $\frac{\Delta R}{R}^{C_4}$, the instantaneous Kerr signal shows a strong enhancement below T_c in the $\frac{\Delta R}{R}^{nem}$ channel. Using the fitting procedure displayed in Figure 2(f,h), we obtained the amplitude of the instantaneous Kerr and decaying components (See Figure 3(b) and ⁴⁶). Interestingly, the channel dependence of the instantaneous Kerr and decaying signal are distinct: while the instantaneous Kerr signal is fully nematic with no C_4 symmetric component within our experimental accuracy, the decaying signal is present in both channels with similar amplitudes at all temperatures ⁴⁶.

Origin of the nematic response The complete switch from C_4 symmetric to nematic channel of the instantaneous Kerr signal when going from the C_4 SC phase to the C_2 SC phase is the central finding of the present work. It indicates an unanticipated and profound impact of the C_4 symmetry breaking on the THz Kerr non-linear optical signal of the SC state. We now explore different scenarios to explain this phenomena. First since the structural transition from tetragonal to orthorhombic involves a mixing of the A_{1g} and B_{1g} symmetry into the A_g symmetry, we naturally expect some mixing of the $\frac{\Delta R}{R}$ symmetry components due to the anisotropy of the optical

constants. Based on optical measurements on detwinned BaFe₂As₂ samples^{46,55}, we determined quantitatively how the two symmetries are mixed from the calculation of the $\frac{1}{R} \frac{\delta R}{\delta \epsilon_1}$ pre-factor in Equation 1. We found at most a 25% anisotropy with respect to the a and b axes. As expected this anisotropy causes a non-zero nematic component. However, it leads to a $\frac{\Delta R}{R}^{nem}$ signal of at most 10% of the $\frac{\Delta R}{R}^{C_4}$ signal, and therefore plays a marginal role in the C_4 symmetric to nematic transition observed in the THz Kerr signal.

Having ruled out a simple effect of anisotropic linear optical constant, we are left with the properties of the non-linear response $\chi^{(3)}$ itself. In the C_2 phase, the anisotropy of the electronic dispersion relation will also induce a non-zero component of the Higgs mode response in the nematic channel³⁷. We evaluated the activation of the Higgs response in the nematic channel by calculating the third-order non-linear Higgs response (See Fig. 3(c,d) for the contribution of the hole pockets) using a three pocket model (2 hole-like and 1 electron-like) and an s-wave superconducting gap⁴⁶. As expected, in the C_4 phase the Higgs response appears below T_c only in the C_4 symmetric channel in agreement with our observations in the UD37 sample. In the C_2 phase however, the distorted Fermi pockets due to finite nematic order parameter activate the Higgs mode in the nematic channel as observed experimentally. The activation grows with the nematic splitting energy Δ_{nem} , but quickly saturates and decreases (See inset of Fig. 3(d)). We found that for any realistic nematic splitting energy and band parameters, the nematic response of either hole or electron pockets is at most 60% of the C_4 symmetric response, thus failing to explain the experimental observation. We note that a dominant contribution from CDF to the THz would be inconsistent with both the fully C_4 symmetric Kerr signal observed in UD37 and the fully nematic Kerr signal

observed in UD26 (see ⁴⁶ for an evaluation of the CDF contribution).

Discussion

From the above discussion, it appears that the strong dominance of the THz Kerr signal in the nematic channel of UD26 cannot be explained simply by the effect of the anisotropy of the optical constant or the electronic structure on the Higgs signal. We are thus left with more speculative scenarios. First, we discuss the possibility of the an exotic SC order parameter in the C_2 phase. We note that an SC order parameter with lower symmetry like d -wave will not by itself activate a Higgs Kerr signal in non-fully symmetric channels as demonstrated in the case of cuprates ^{37,42}, so that our observations cannot be easily linked to a change in SC gap symmetry at least for a single band superconductor. However, in multi-orbital systems like Fe superconductors it is possible that the internal structure of Cooper pairs in orbital space profoundly affects the anisotropy of the Kerr Higgs signal. An intriguing possibility is the recent proposal of an orbital-selective SC state in the C_2 phase of FeSe ¹³. Whether such state would by itself yield a Higgs signal in the nematic channel only is unclear and deserves further theoretical investigations.

Another possibility is that the THz Kerr signal arises from an SC collective mode which couples to the nematic order parameter. In $\text{Ba}_{1-x}\text{K}_x\text{Fe}_2\text{As}_2$ s and d wave pairing channels are close competitors, potentially giving rise to a Bardasis-Schrieffer (BS) mode in the nematic d wave channel ^{10,56,57}. Several spectral features of the Raman spectrum of $\text{Ba}_{1-x}\text{K}_x\text{Fe}_2\text{As}_2$ have indeed been interpreted as BS modes, consistent with theoretical evaluations of pairing instabilities in

hole-doped BaFe_2As_2 ^{10,11,58,59} (see also SM for a discussion of the Raman spectra in the SC state). Recently, Muller et al. have argued that in the C_2 phase the BS mode will couple to the amplitude mode of the nematic order parameter, giving rise to a single coupled nematic-BS mode below the Higgs mode energy due to the appearance of a strongly mixed $s+d$ SC state²⁴. The stronger decaying signal in the UD26 sample compared to the UD37 sample well-below T_c supports the idea of an increased anisotropy of the SC gap in the C_2 SC phase in agreement with a significant d wave admixture. Interestingly, for parameters close to the critical point where the nematic phase terminates Muller et al. found that the coupled nematic-BS mode may become dominant over the Higgs mode in the short times dynamics after a quench²⁴. Furthermore, we note that the BS mode has the nematic B_{1g} symmetry and will naturally give rise to a signal in the nematic channel⁶⁰. A computation of the third-order non-linear susceptibility taking into account both s and d pairing channels in the presence of a finite nematic order parameter is desirable to further assess this scenario.

In conclusion, we have studied the impact of nematicity on the SC collective modes in $\text{Ba}_{1-x}\text{K}_x\text{Fe}_2\text{As}_2$ via THz pump optical probe measurements. In the absence of nematicity we observe an instantaneous behavior of the optical reflectivity which we assign to a THz Kerr coupling to the Higgs mode. In the coexisting nematic + SC phase we observe a drastic change in the polarization dependence of the THz Kerr signal from purely C_4 symmetric to purely nematic. The change cannot be accounted by the anisotropy of the electronic properties and indicates the emergence of a new SC collective mode which couples strongly to the nematic order parameter. The exact identification of this mode requires further investigation, but we suggest the Bardasis-Schrieffer

mode connecting nearly-degenerate s and d wave pairing ground states as a likely candidate.

Methods

Samples. The two single crystals of $\text{Ba}_{1-x}\text{K}_x\text{Fe}_2\text{As}_2$ with $T_c = 26\text{K}$ (UD26, $x \sim 0.23$) and $T_c = 37\text{K}$ (UD37, $x \sim 0.28$) were characterized by SQUID magnetometry, wavelength dispersing spectroscopy and Raman scattering measurements. The samples are square-shaped with sides of $\sim 5\text{ mm}$. The crystal orientations of both samples were confirmed by polarization-resolved Raman spectroscopy measurements.

Terahertz pump-optical reflectivity probe (TPOP). Strong single cycle THz pump pulses (0.3 - 1 THz) with electric field reaching up to 350 kV/cm are generated using optical rectification of 1.5 eV NIR pulses in a LiNbO_3 crystal using the tilted pulse front technique^{61,62}. For optical probe measurements 100 fs duration NIR pulses at 1.5 eV are used with a fluence of 10-100 nJ/cm² and a spot size of 250 μm in diameter. The repetition rate of the NIR laser is 1kHz.

Data availability

The authors declare that [the/all other] data supporting the findings of this study are available within the paper [and its supplementary information files].

Code availability

All the numerical codes that support the findings of this study are available from the corresponding authors (R.G., Y. G. and R.S.) upon reasonable request.

Acknowledgements

The authors would like to thank M. Müller, I. Eremin, R. Lobo, I. Paul and L. Benfatto for fruitful discussions. R. G. and Y. G. acknowledge the support from the Japan Society for the Promotion of Science.

Competing Interests:

the Authors declare no Competing Financial or Non-Financial Interests.

Author contributions

The samples were grown by H-H.W. and X-H.C.; R.G. and K.K. performed THz pump optical probe experiments; P. M. performed Raman experiments; R.G. and Y.G. performed the calculations and analyzed data; Y.G. and R. S. supervised the project; All authors discussed the results and wrote the manuscript.

Correspondence:

Correspondence should be addressed to R. Grasset (email: romain.grasset@polytechnique.edu), Y. Gallais (email: yann.gallais@u-paris.fr) and R. Shimano (email: shimano@thz.phys.s.u-tokyo.ac.jp).

References

1. Fradkin, E., Kivelson, S. A. & Tranquada, J. M. *Colloquium* : Theory of intertwined orders in high temperature superconductors. Reviews of Modern Physics **87**, 457–482 (2015).
2. Fernandes, R. M., Chubukov, A. V. & Schmalian, J. What drives nematic order in iron-based superconductors? Nat. Phys. **10**, 97–104 (2014).
3. Yonezawa, S. et al. Thermodynamic evidence for nematic superconductivity in $\text{Cu}_x\text{Bi}_2\text{Se}_3$. Nature Physics **13**, 123–126 (2017).
4. Kerelsky, A. et al. Maximized electron interactions at the magic angle in twisted bilayer graphene. Nature **572**, 95–100 (2019).
5. Cao, Y. et al. Nematicity and competing orders in superconducting magic-angle graphene. Science **372**, 264–271 (2021).
6. Canfield, P. C. & Bud'ko, S. L. FeAs-based superconductivity: A case study of the effects of transition metal doping on BaFe_2As_2 . Annu. Rev. Condens. Matter Phys. **1**, 27–50 (2010).
7. Chu, J.-H., Kuo, H.-H., Analytis, J. G. & Fisher, I. R. Divergent nematic susceptibility in an iron arsenide superconductor. Science **337**, 710–712 (2012).

8. Gallais, Y. et al. Observation of incipient charge nematicity in $\text{Ba}(\text{Fe}_{1-x}\text{Co}_x)_2\text{As}_2$. Phys. Rev. Lett. **111**, 267001 (2013).
9. Böhmer, A. E. et al. Superconductivity-induced re-entrance of the orthorhombic distortion in $\text{Ba}_{1-x}\text{K}_x\text{Fe}_2\text{As}_2$. Nat. Commun. **6**, 7911 (2015).
10. Graser, S., Maier, T. A., Hirschfeld, P. J. & Scalapino, D. J. Near-degeneracy of several pairing channels in multiorbital models for the Fe pnictides. New J. Phys. **11**, 025016 (2009).
11. Böhm, T. et al. Microscopic origin of Cooper pairing in the iron-based superconductor $\text{Ba}_{1-x}\text{K}_x\text{Fe}_2\text{As}_2$. npj Quantum Mater. **3**, 48 (2018).
12. Fernandes, R. M. & Millis, A. J. Nematicity as a probe of superconducting pairing in iron-based superconductors. Phys. Rev. Lett. **111**, 127001 (2013).
13. Sprau, P. O. et al. Discovery of orbital-selective Cooper pairing in FeSe. Science **357**, 75–80 (2017).
14. Littlewood, P. B. & Varma, C. M. Amplitude collective modes in superconductors and their coupling to charge-density waves. Phys. Rev. B **26**, 4883–4893 (1982).
15. Moor, A., Volkov, P. A., Volkov, A. F. & Efetov, K. B. Dynamics of order parameters near stationary states in superconductors with a charge-density wave. Phys. Rev. B **90**, 024511 (2014).
16. Fu, W., Hung, L.-Y. & Sachdev, S. Quantum quenches and competing orders. Phys. Rev. B **90**, 024506 (2014).

17. Raines, Z. M., Stanev, V. G. & Galitski, V. M. Hybridization of Higgs modes in a bond-density-wave state in cuprates. Phys. Rev. B **92**, 184511 (2015).
18. Dzero, M., Khodas, M. & Levchenko, A. Amplitude modes and dynamic coexistence of competing orders in multicomponent superconductors. Phys. Rev. B **91**, 214505 (2015).
19. Gallais, Y., Paul, I., Chauvière, L. & Schmalian, J. Nematic Resonance in the Raman Response of Iron-Based Superconductors. Phys. Rev. Lett. **116**, 017001 (2016).
20. Soto-Garrido, R., Wang, Y., Fradkin, E. & Cooper, S. L. Higgs modes in the pair density wave superconducting state. Phys. Rev. B **95**, 214502 (2017).
21. Sentef, M. A., Tokuno, A., Georges, A. & Kollath, C. Theory of laser-controlled competing superconducting and charge orders. Phys. Rev. Lett. **118**, 087002 (2017).
22. Morice, C., Chakraborty, D. & Pépin, C. Collective mode in the SU(2) theory of cuprates. Physical Review B **98**, 224514 (2018).
23. Müller, M. A., Volkov, P. A., Paul, I. & Eremin, I. M. Collective modes in pumped unconventional superconductors with competing ground states. Phys. Rev. B **100**, 140501(R) (2019).
24. Müller, M. A., Volkov, P. A., Paul, I. & Eremin, I. M. Interplay between nematicity and Bardasis-Schrieffer modes in the short-time dynamics of unconventional superconductors. Phys. Rev. B **103**, 024519 (2021).
25. Pekker, D. & Varma, C. Amplitude/Higgs modes in condensed matter physics. Annu. Rev. Condens. Matter Phys. **6**, 269–297 (2015).

26. Shimano, R. & Tsuji, N. Higgs mode in superconductors. Annu. Rev. Condens. Matter Phys. **11**, 103–124 (2020).
27. Sooryakumar, R. & Klein, M. V. Raman scattering by superconducting-gap excitations and their coupling to charge-density waves. Phys. Rev. Lett. **45**, 660–662 (1980).
28. Méasson, M.-A. et al. Amplitude Higgs mode in the 2H-NbSe₂ superconductor. Phys. Rev. B **89**, 060503(R) (2014).
29. Grasset, R. et al. Higgs-mode radiance and charge-density-wave order in 2H-NbSe₂. Phys. Rev. B **97**, 094502 (2018).
30. Grasset, R. et al. Pressure-induced collapse of the charge density wave and higgs mode visibility in 2H-TaS₂. Phys. Rev. Lett. **122**, 127001 (2019).
31. Tsuji, N. & Aoki, H. Theory of Anderson pseudospin resonance with Higgs mode in superconductors. Phys. Rev. B **92**, 064508 (2015).
32. Cea, T., Castellani, C. & Benfatto, L. Nonlinear optical effects and third-harmonic generation in superconductors: Cooper pairs versus Higgs mode contribution. Phys. Rev. B **93**, 180507(R) (2016).
33. Murotani, Y. & Shimano, R. Nonlinear optical response of collective modes in multiband superconductors assisted by nonmagnetic impurities. Phys. Rev. B **99**, 224510 (2019).

34. Udina, M., Cea, T. & Benfatto, L. Theory of coherent-oscillations generation in terahertz pump-probe spectroscopy: From phonons to electronic collective modes. Phys. Rev. B **100**, 165131 (2019).
35. Tsuji, N. & Nomura, Y. Higgs-mode resonance in third harmonic generation in NbN superconductors: Multiband electron-phonon coupling, impurity scattering, and polarization-angle dependence. Phys. Rev. Research **2**, 043029 (2020).
36. Seibold, G., Udina, M., Castellani, C. & Benfatto, L. Third harmonic generation from collective modes in disordered superconductors. Phys. Rev. B **103**, 014512 (2021).
37. Schwarz, L. & Manske, D. Theory of driven Higgs oscillations and third-harmonic generation in unconventional superconductors. Phys. Rev. B **101**, 184519 (2020).
38. Matsunaga, R. et al. Higgs amplitude mode in the bcs superconductors $\text{Nb}_{1-x}\text{Ti}_x\text{N}$ induced by terahertz pulse excitation. Phys. Rev. Lett. **111**, 057002 (2013).
39. Matsunaga, R. et al. Light-induced collective pseudospin precession resonating with Higgs mode in a superconductor. Science **345**, 1145–1149 (2014).
40. Matsunaga, R. et al. Polarization-resolved terahertz third-harmonic generation in a single-crystal superconductor NbN: Dominance of the Higgs mode beyond the BCS approximation. Phys. Rev. B **96**, 020505(R) (2017).
41. Nakamura, S. et al. Infrared activation of the Higgs mode by supercurrent injection in superconducting NbN. Phys. Rev. Lett. **122**, 257001 (2019).

42. Katsumi, K. et al. Higgs mode in the *d*-wave superconductor $\text{Bi}_2\text{Sr}_2\text{CaCu}_2\text{O}_{8+x}$ driven by an intense terahertz pulse. Phys. Rev. Lett. **120**, 117001 (2018).
43. Chu, H. et al. Phase-resolved Higgs response in superconducting cuprates. Nat. Commun. **11**, 1793 (2020).
44. Yang, X. et al. Lightwave-driven gapless superconductivity and forbidden quantum beats by terahertz symmetry breaking. Nat. Photonics **13**, 707–713 (2019).
45. Vaswani, C. et al. Light quantum control of persisting Higgs modes in iron-based superconductors. Nat. Commun. **12**, 258 (2021).
46. See Supplementary Materials.
47. Hoffmann, M. C., Brandt, N. C., Hwang, H. Y., Yeh, K.-L. & Nelson, K. A. Terahertz Kerr effect. Appl. Phys. Lett. **95**, 231105 (2009).
48. Yang, X. et al. Lightwave-driven gapless superconductivity and forbidden quantum beats by terahertz symmetry breaking. Nature Photonics **13**, 707–713 (2019).
49. Boyd, R. W. Nonlinear Optics 3 (Academic Press, Inc., Boston, 2008).
50. Paul, I. Nonlinear terahertz electro-optical responses in metals. Preprint at <http://arxiv.org/abs/2101.04136> (2021).
51. Cea, T., Barone, P., Castellani, C. & Benfatto, L. Polarization dependence of the third-harmonic generation in multiband superconductors. Phys. Rev. B **97**, 094516 (2018).

52. Silaev, M. Nonlinear electromagnetic response and Higgs-mode excitation in BCS superconductors with impurities. Phys. Rev. B **99**, 224511 (2019).
53. Jujo, T. Quasiclassical theory on third-harmonic generation in conventional superconductors with paramagnetic impurities. J. Phys. Soc. Jpn. **87**, 024704 (2018).
54. Thewalt, E. et al. Imaging anomalous nematic order and strain in optimally doped $\text{BaFe}_2(\text{As}, \text{P})_2$. Phys. Rev. Lett. **121**, 027001 (2018).
55. Nakajima, M. et al. Unprecedented anisotropic metallic state in undoped iron arsenide BaFe_2As_2 revealed by optical spectroscopy. PNAS **108**, 12238 (2011).
56. Bardasis, A. & Schrieffer, J. R. Excitons and plasmons in superconductors. Physical Review **121**, 1050–1062 (1961).
57. Barlas, Y. & Varma, C. M. Amplitude or Higgs modes in d-wave superconductors. Phys. Rev. B **87**, 054503 (2013).
58. Maiti, S. & Hirschfeld, P. J. Collective modes in superconductors with competing s - and d -wave interactions. Phys. Rev. B **92**, 094506 (2015).
59. Maiti, S., Maier, T. A., Böhm, T., Hackl, R. & Hirschfeld, P. J. Probing the pairing interaction and multiple Bardasis-Schrieffer modes using Raman spectroscopy. Phys. Rev. Lett. **117**, 257001 (2016).
60. Müller, M. A. & Eremin, I. M. Signatures of Bardasis-Schrieffer mode excitation in third-harmonic generated currents. Preprint at <http://arxiv.org/abs/2107.02834> (2021).

61. Hebling, J., Yeh, K.-L., Hoffmann, M. C., Bartal, B. & Nelson, K. A. Generation of high-power terahertz pulses by tilted-pulse-front excitation and their application possibilities. J. Opt. Soc. Am B **25**, B6–B19 (2008).
62. Watanabe, S., Minami, N. & Shimano, R. Intense terahertz pulse induced exciton generation in carbon nanotubes. Opt. Express **19**, 1528–1538 (2011).

Figure legends

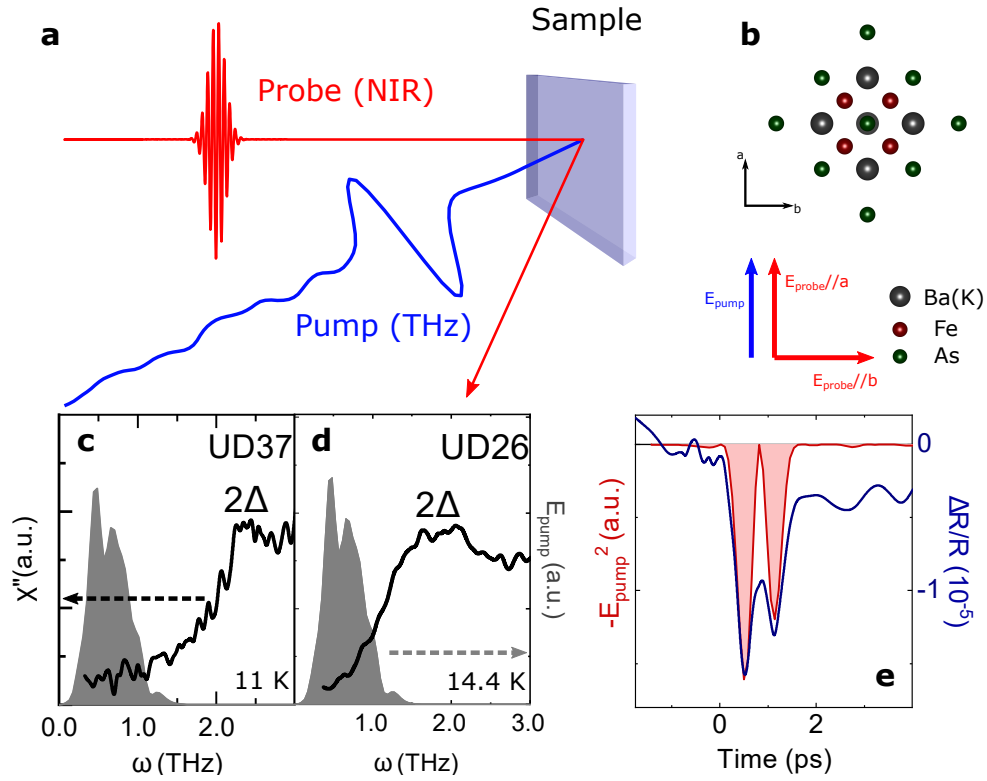


Figure 1: **Non linear THz response in $\text{Ba}_{1-x}\text{K}_x\text{Fe}_2\text{As}_2$.** (a) Sketch of the THz pump near-infrared (NIR) probe measurements. (b) Crystal structure of BaFe_2As_2 and the two polarization configurations used to determine the C_4 symmetric and nematic components of the transient reflectivity. (c,d) Raman spectra of $\text{Ba}_{1-x}\text{K}_x\text{Fe}_2\text{As}_2$ in the B_{1g} symmetry for UD37 (c) and UD26 (d) below T_c . 2Δ indicates superconducting gap from the hole pockets. The grey curve represents the energy spectrum of the THz pump. (e) For UD37, $\Delta R/R$ (blue line) along one of the Fe-Fe axis at 20 K ($T < T_c$) as a function of delay time between the pump and probe pulses. The E_{pump}^2 (red line) component corresponds to the THz Kerr effect.

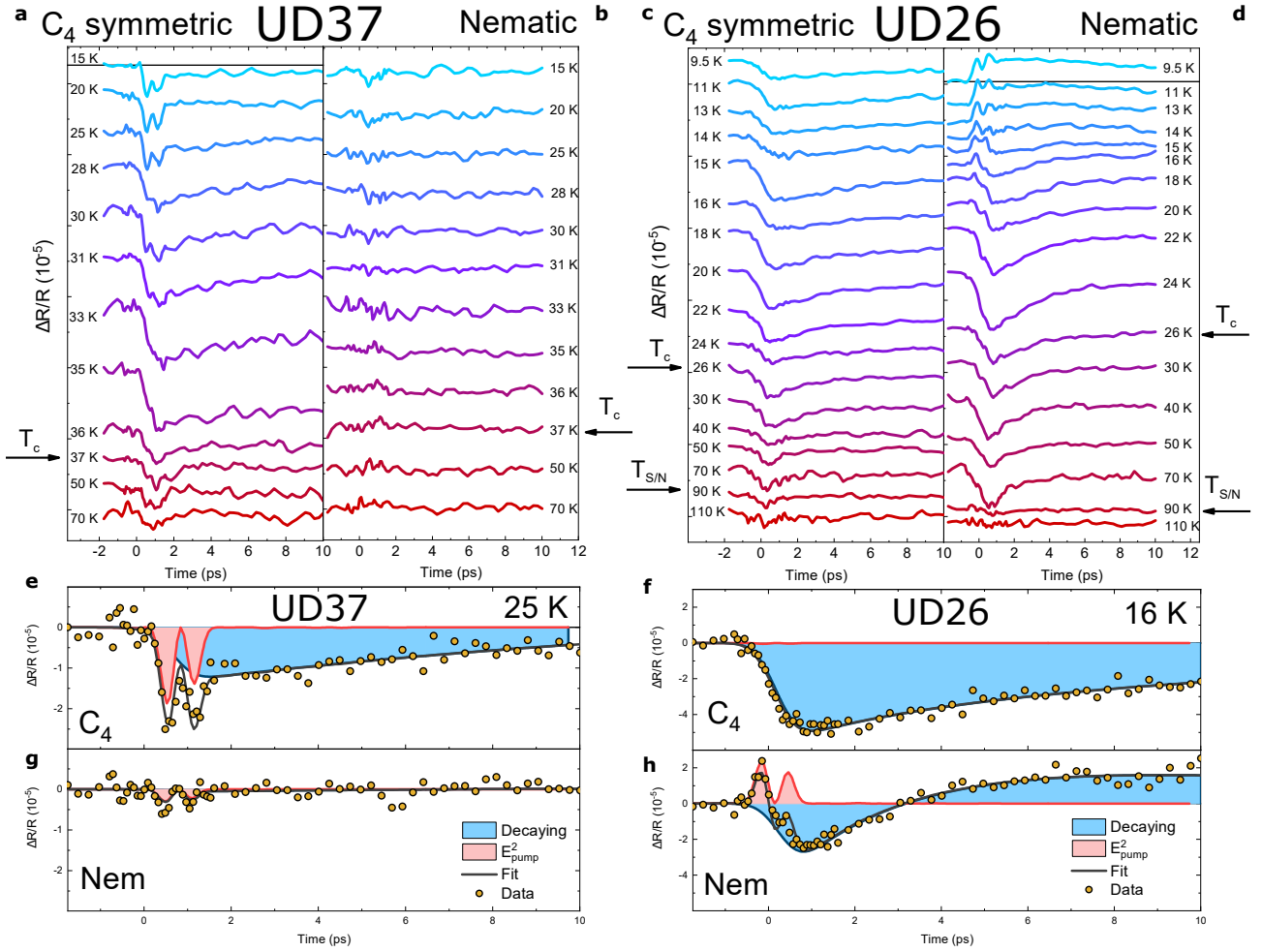


Figure 2: **Temperature and symmetry dependence of the THz response.** (a-d) $\Delta R/R$ against the delay time in the C_4 symmetric (C_4) and nematic (Nem) channels at various temperatures for UD37 (a,b) and UD26 (c,d). (e-h) Fitted curves for the different components of $\frac{\Delta R}{R}$ at $T < T_c$ for UD37 (e,g) and UD26 (f,h).

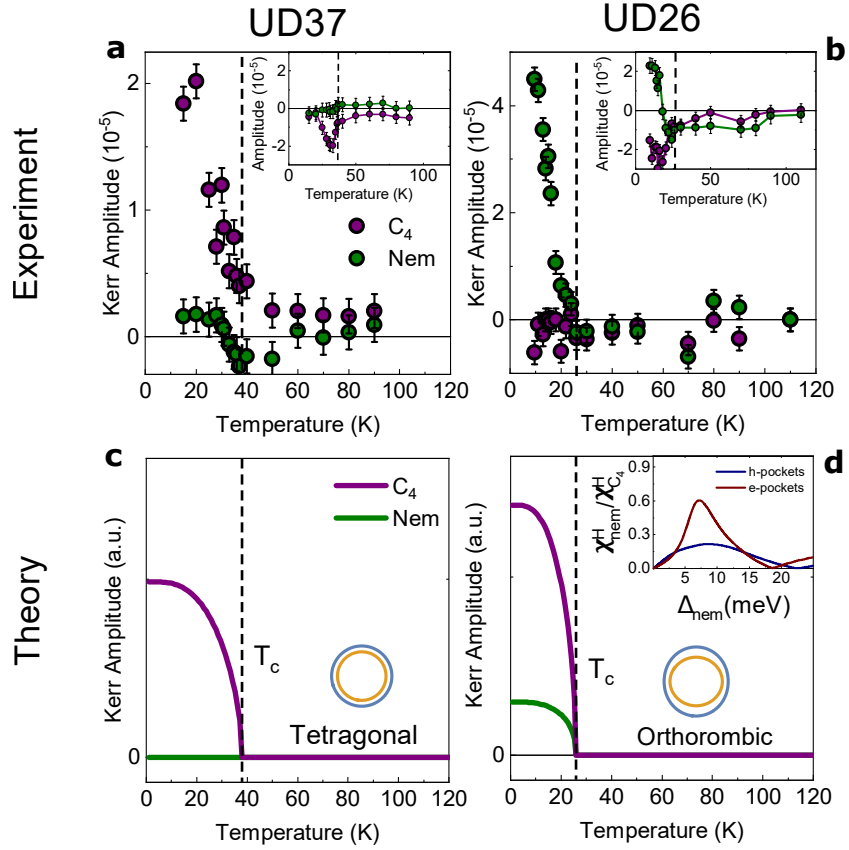


Figure 3: **Instantaneous Kerr response** (a,b) Temperature dependencies of the amplitude of the fitted instantaneous Kerr signals in the C_4 symmetric (C_4) and nematic (nem) channels for UD37 (a) and UD26 (b). Insets: Temperature dependencies of the amplitude of the fitted SC decaying signals. (c,d) Calculated temperature dependence of Higgs contribution of the hole pockets to the instantaneous Kerr signals in the C_4 symmetric (C_4) and nematic (nem) channels for a tetragonal (c) and orthorhombic (d) symmetry of the electronic dispersion relation. The shape of the Fermi surfaces of our model is represented in blue and yellow. Inset: Ratio of the nematic and C_4 symmetric components of the Higgs response as a function of the nematic order parameter for the hole (blue) and electron pockets (red).